Atmos. Meas. Tech. Discuss., 3, 4675–4705, 2010
www.atmos-meas-tech-discuss.net/3/4675/2010/
doi:10.5194/amtd-3-4675-2010

Atmospheric Measurement Techniques Discussions

LIDAR technology for measuring trace gases on Mars and Earth

H. Riris[1], K. Numata[2], S. Li[1], S. Wu[1], X. Sun[1], and J. Abshire[1]

[1]NASA Goddard Space Flight Center, Greenbelt, MD 20771, USA
[2]University of Maryland, Department of Astronomy, College Park, MD 20742, USA

Received: 1 October 2010 – Accepted: 8 October 2010 – Published: 2 November 2010

Correspondence to: H. Riris (haris.riris@nasa.gov)

Published by Copernicus Publications on behalf of the European Geosciences Union.

Abstract

Trace gases and their isotopic ratios in planetary atmospheres offer important but subtle clues as to the origins of a planet's atmosphere, hydrology, geology, and potential for biology. Calculations show that an orbiting laser remote sensing instrument is capable of measuring trace gases on a global scale with unprecedented accuracy, and higher spatial resolution that can be obtained by passive instruments. Our proposed lidar uses Integrated Path Differential Absorption technique, Optical Parametric Amplifiers, and a receiver with high sensitivity detector at 1.65 µm to map methane concentrations, a strong greenhouse gas. For Mars we can use the same technique in the 3–4 µm spectral range to map various biogenic gas concentrations and search for the existence of life. Preliminary results demonstrating methane and water vapour detection using a laboratory prototype illustrate the viability of the technique.

1 Introduction

Methane is the second most important anthropogenically produced greenhouse gas. Though its atmospheric abundance is lower than that of CO_2 (1.78 ppm vs. 380 ppm) it has a 23 times larger (see IPCC report 2007) greenhouse heating potential. Methane also contributes to pollution in the lower atmosphere through chemical reactions leading to ozone production. Atmospheric methane concentrations are highly variable and have been increasing as a result of increased fossil fuel production, rice farming, livestock and landfills. Natural sources of methane include wetlands, wild fires, and termites and perhaps other unknown but significant sources (Keppler et al., 2006). Vast amounts of methane are contained in the continental shelf in the form of methane hydrates. Important sinks for methane include non-saturated soils and oxidation by hydroxyl radicals in the atmosphere. Trends in atmospheric methane concentrations have been highly variable over the last two decades and the reasons are still poorly

AMTD
3, 4675–4705, 2010

understood. Better knowledge of atmospheric methane distribution and fluxes are needed for a correct assessment of its impact on global change (Houghton et al., 2001). NASA's Decadal Survey for the Active Sensing of CO_2 Emissions Over Nights, Days, and Seasons (ASCENDS) mission recognized the importance of methane and stated that: "Ideally, to close the carbon budget, methane should also be addressed, but the required technology is not now obvious. If appropriate and cost-effective methane technology becomes available, methane capability should be added" (National Research Council Decadal Survey, 2007).

Our observations of greenhouse gases have been previously limited to in-situ (surface and tower sites) and sparse airborne measurements. Since 2009 space measurements have become available from the JAXA GOSAT mission (see for example Hamazaki et al., 2007 and Yokota et al., 2009). More global observations are urgently needed in order to better understand climate forcings and to reduce the uncertainty in the carbon budget. Several greenhouse gases must be measured in order to understand the complete carbon budget. Methane levels have remained relatively constant over the last decade around 1.78 parts per million (ppm) (Dlugokencky et al., 2003) but recent observations have indicated that levels may be on the rise. The underlying causes for these trends are still uncertain. One hypothesis is that vast reservoirs of methane are trapped in the permafrost regions of North America, Europe, and Siberia and as global temperatures rise large amounts of methane will be released into the atmosphere (Christensen, 2004). Another hypothesis points to increased production of methane by methanogenic microbes as the permafrost warms up and temperatures rise.

Methanogenic microbes or other extremophiles may be present below the surface on other planets. Habitable environments are believed to have existed in the past on Mars and could potentially persist today. Thus, the ability to make well-resolved measurements of CH_4, and its isotopes in planetary atmospheres is important. However, inorganic processes can also produce trace gases, such as CH_4, that may be mistaken for biogenic markers. These processes involve the out-gassing of primordial components,

AMTD
3, 4675–4705, 2010

comet impacts, and reactions with volcanic rock in hydrothermal systems. To distinguish organic from inorganic sources will require quantitative regional and temporal concentration estimates of traces gases.

Trace gases have been measured in the Mars atmosphere from Earth, Mars orbit, and in-situ on the Martian surface. Recent planetary missions and ground based observations (Smith, 2008; Mumma, 2004, 2009) have provided strong evidence of reservoirs of methane and water on Mars (Smith, 2009) which could potentially harbor life. The observations suggested large seasonal and spatial variations of methane concentrations in the Martian atmosphere.

The atmosphere of Mars is surprisingly dynamic with various processes driving changes in the distribution of CO_2, dust, haze, clouds and water vapor on global scales (Kahn, 1992). The Mars atmosphere exchanges nearly 30% of its mass with the solid surface annually. This process consists of precipitation and sublimation of solid CO_2. To fully resolve its components and activity, requires high spatial resolution. Some processes, such as polar cloud formation, also occur at night, and which are invisible to most passive sensors. A lidar that can accurately quantify trace gases in planetary atmospheres, localize their sources and variability, and determine their lifetime can observe these processes and help answer questions about planetary evolution, and potential for life.

2 Measurement approach and technology

In order to measure remotely trace gases, two primary components are needed: a tunable transmitter with sufficient energy, whose spectral emission will overlap the gas absorption lines; a receiver with a sensitive detector to detect the reflected laser energy. Many trace gas molecules of interest have their fundamental absorption bands in the 3–4 µm region, thus using a transmitter in this region will significantly enhance the sensitivity of the measurement. The molecular overtone bands in the near infrared region may be more suitable in cases where multiple species interfere with each other

AMTD
3, 4675–4705, 2010

or if the lines are so strong they completely absorb the laser radiation.

Methane has absorptions in most of the near and mid-IR spectral range. The strongest bands are at 1.65, 2.2., 3.3 and 7.8 µm. The band at 3.3 µm is the strongest and is ideal for making high sensitivity measurements of methane in low-pressure planetary atmospheres, such as Mars. The average surface pressure is ~6–7 mbar, which minimizes pressure broadening and results in narrow absorption lines. For example, the Doppler width of a CH_4 line at 3057.726 cm^{-1} (3270.404 nm) is 0.0079 cm^{-1} (237 MHz). A very high resolution FTIR spectrometer with a resolution of ~0.03 cm^{-1} (900 MHz), is more than three times the width of the CH_4 line. By comparison a laser spectrometer could have 0.000033 cm^{-1} (1 MHz) resolution and therefore sensitivity. Measurements from passive spectrometers in the mid-infrared are also restricted to the sunlit side of a planet, generally in the mid latitudes. To map the global distribution of these gases, requires an instrument with high sensitivity and spatial and spectral resolution that also has global coverage measuring during both day and night.

Figure 1 shows the expected atmospheric transmission from 3.0 to 4.0 µm and Fig. 2 the shows the expected methane absorption at 3.270 µm through the Martian atmosphere from an orbit of 400 km. A uniform 10 parts per billion (ppb) volume mixing ratio was assumed for methane in Fig. 2.

In contrast, the 3.3 µm spectral region is not well suited for methane measurements in the Earth's atmosphere. The CH_4 lines in this wavelength region are too strong and will completely absorb the laser radiation in a few hundreds of meters. There is also significant interference from water vapor thus making any accurate measurements of methane extremely difficult. The near infrared overtones of CH_4 at 1.65 µm are almost two orders of magnitude weaker than those at 3.3 µm, but they are relatively free of interference from other atmospheric species and are well suited for remote sensing of methane on Earth. Figure 3 shows the calculated one way transmittance from an altitude of 450 km through the earth's atmosphere at 1.651 µm. The candidate methane lines are strong enough to be used for lidar observations with very little interference from other species, including water.

AMTD
3, 4675–4705, 2010

Both of these spectral regions (3–4 µm and 1.65 µm) are accessible with a laser using Optical Parametric Generation (OPG). In OPG, a photon of an incident laser pulse (pump) is divided into two photons by a nonlinear optical crystal. When the pump power is high enough any photons that satisfy the energy and phase matching conditions are converted. Optical Parametric Amplifiers (OPA) are a seeded version of OPG. Laser light from a signal beam propagates through a nonlinear crystal together with a pump beam of shorter wavelength and the seed signal is amplified and an idler is generated. The wavelength of the idler photons is the difference between the seed and the pump. Finally an Optical Parametric Oscillator (OPO) can be regarded as an OPA with optical feedback. The nonlinear crystal is placed inside a cavity just like a laser crystal in a laser resonator cavity. The differences between these methods are illustrated in Fig. 4.

Our current breadboard experiment uses the OPA approach and is shown in Fig. 5. A nonlinear periodically poled Lithium Niobate (PPLN) crystal is pumped by a pulsed 1064 nm Nd:YAG 1064 nm and seeded by a continuous-wave (CW) ~1.6 µm diode laser. The pump source is a passively Q-switched, Nd:YAG non-planar ring oscillator (NPRO) made by Innolight Inc. that emits a single-frequency output at 1064.5 nm. It has a 3.3-ns pulse width and maximum energy of 60-µJ per pulse at a 6-kHz repetition rate. The typical energy coupled into the crystal for conversion is ~42 µJ. The laser is operating in single mode and its optical linewidth is transform limited (~133 MHz). The seed source is a CW, fiber-coupled, distributed-feedback (DFB) laser diode. The wavelength of the laser diode is selected to be between 1530 nm and 1660 nm depending on target trace gas. The laser diode is smoothly tuned across the absorption peak of the target gas. The linewidth of the diode is less than 1 MHz. The OPA crystal is 50-mm long, 1-mm thick, MgO-doped PPLN with 4 grating channels (30.0–31.5 µm). The end surfaces of the crystal were angled at 5° and AR coated at the pump, the signal and the idler wavelengths, in order to minimize optical feedback and etalon fringes. The temperature of the crystal is tuned between 70 °C and 170 °C to optimize the phase matching at the target wavelength. The output beam is separated into three paths

AMTD
3, 4675–4705, 2010

depending on wavelengths using dichroic mirrors. The signal and the idler are used for gas detection through a gas cell or through an open-path. The signal and the idler are detected by InGaAs and HgCdZnTe detectors, respectively and the signals are averaged by a boxcar averager and digitzed for processing and display.

3 OPA performance and signal to noise ratio

3.1 OPA tuning range, output energy, and efficiency

A very important parameter for a lidar is its tuning range. Figure 6 shows the present tuning range of our system which we can achieve by changing the crystal's grating period and temperature. The center wavelength of the unseeded OPG spectra was tuned from 1520 nm to 1770 nm. The corresponding tuning range of the idler output was 2670 nm ~3550 nm. The full-width half-maximum of the unseeded OPG spectra was about 2 nm at 1578.2 nm. Once seeded within the gain bandwidth, the output spectrum followed the seed wavelength linewidth with > 20 dB suppression.

The maximum energy we have achieved with the present setup is ~10.0 μJ and it was limited by the pump laser. Increasing the pump should increase the signal and idler pulse energies and it will also improve the detection sensitivity of the lidar instrument. Figure 7 shows the relationship between signal and pump energy, and Fig. 8 shows the signal energy vs. seed power for a fixed pump power. The maximum power we obtained with a 42-μJ pump and a 393-mW seed at 1578.2 nm, was ~10.8-μJ signal energy and ~5.2 μJ of idler energy. Thus, the total optical conversion efficiency was (10.8 μJ + 5.2 μJ)/42 μJ ~38%. When there was no back conversion, the relationship agreed well with theory (blue curve in Fig. 7). With a more efficient pump source the overall efficiency of the laser transmitter can be as high as 10%.

AMTD
3, 4675–4705, 2010

4 Experimental results

4.1 Detection of methane, water vapor, and carbon dioxide at 3.3 µm

After optimizing our system for 3.3 µm we demonstrated methane detection in a cell. Figure 9 shows the results of the scans with the optimized system at two different energy levels for the OPA and comparison with the theoretical spectrum as calculated from the HITRAN data base. Even at high power (~6.95 µJ/pulse) the agreement between theory and experiment is excellent. Figure 10 shows water vapor spectra at ~2.996 µm at various pressures through the cell.

In our setup (Fig. 5) we get both the idler and the amplified seed wavelengths. Our seed wavelength is 1.578 µm which is coincident with a near CO_2 absorption. In fact, both methane and CO_2 absorptions can be scanned simultaneously (Fig. 11). This is a clear demonstration of the use of the OPA at two different wavelength ranges and also illustrates the the capability of the instrument to measure more than one trace gas line with a single laser. This feature could be especially useful for Mars where simultaneous measurements of methane and carbon dioxide could be very beneficial. Even though this is not the optimum (strongest) CO_2 line it can still be easily used on Mars, since 95% of the Martian atmosphere is composed of CO_2.

Detection of methane on Mars requires high sensitivities on the order of 1 ppb. In most spectrometers the limiting noise source is usually not random noise but other instrumental effects, such as etalon fringes (see for example Werle et.al. 1993). We performed a series of experiments to establish the minimum detectable absorption of our spectrometer. Figure 12 shows methane measurements in a cell at two different pressures (0.072 and 0.065 Torr) in a 310 mm cell. The methane concentration was 2.91%. Even though there is a baseline structure, probably due to etalon fringes from the PPLN crystal, we can clearly discern the absorption. Etalon fringes are basically interference effects from multiple optical surfaces in the optical path and can be the limiting factor in laser diode spectrometers. Various techniques have been suggested for reducing their impact (Werle, 2004; Bomse, 2006; Riris, 1994). At these pressures

AMTD
3, 4675–4705, 2010

(0.072 and 0.065 Torr) the equivalent methane concentration in ppm was ~2.8 ppm in a 310 mm cell. This translates to a sensitivity of 0.87 ppm/m. By comparison for remote sensing measurements on Mars, where the atmospheric scalenegth is ~11 km for a total pathlength of 22 km, if we want to detect 1 ppb on Mars we must have a sensitivity that exceeds ~22 ppm/m. We obviously meet the detection sensitivity criterion and we are confident with a well engineered instrument we can increase the detection sensitivity limit even further.

These results were repeated and verified with a methane mixture with lower concentration (1000 ppm). Figure 13 shows methane measurements in a cell at two different pressures (2.2 and 1.1 Torr) in a 310 mm (31 cm) cell. The methane concentration was 1000 ppm or 0.1%. Even though there is still a baseline structure we can clearly discern the absorption at 2.0 Torr. Following the same calculations as above, we get a sensitivity of 0.90 ppm/m, which is in close agreement with the earlier result.

For the open path measurements at this wavelength we used a cooperative target overlooking the GSFC parking lot about 200 m away from our lab. The infrared beam was coupled into an infrared fiber, collimated by a 20 cm diameter transmit telescope and sent to a reflective target 200 m away. The reflected beam was collected by a 20 cm diameter telescope and onto an infrared detector made by Boston Electronics (PVMI 10.6).

Figure 14 shows the methane spectra from a 200 m (one way) open path measurement using a reflective target and comparison with HITRAN using 2.5 and 3.0% water vapor concentration. The methane absorption is atmospherically broadened and there is a strong water vapor absorption to the right of the methane line that completely extinguishes the laser. However, it is clear from these results that this technique is applicable to methane monitoring and is capable of achieveing high sensitivities.

4.2 Detection of methane at 1.65 µm

The band at 3.3 µm is the strongest and is ideal for making high sensitivity measurements of methane in low-pressure planetary atmospheres, e.g. Mars. However, this

AMTD
3, 4675–4705, 2010

wavelength region is not well suited for methane earth monitoring. The CH_4 lines in this wavelength region are too strong and will completely absorb the laser radiation in a few hundreds of meters. There is also significant interference from water which is highly variable, thus making any accurate measurements of methane extremely difficult. The near infrared overtones of CH_4 at 1.65 µm are two orders of magnitude weaker than those at 3.3 µm, but they are relatively free of interference from other atmospheric species and are perfectly suited for remote sensing of methane on Earth since they are mostly not completely absorbed. The candidate methane lines are strong enough to be used for laser remote sensing observations with very little interference from other species, including water.

By changing the seed laser we were successful in generating 1.65 µm and measuring methane in a cell and an open path. Figure 15 shows the methane absorption cell at various OPA power levels and a comparison with the expected absorption as calculated from HITRAN in our cell. The agreement between the theory and experiment was excellent and there was no significant degradation as the laser energy was increased.

Ultimately a remote sensing instrument would have to operate from orbit or an airborne platform to make observations of the metahne in the atmosphere. We performed open path measurements at 1650 nm to demonstrate the applicability of this technique. The near-IR beam was coupled into an infrared fiber, collimated by a small transmit beam expander telescope and sent to a reflective target 1.5 km away. The reflected beam was collected by a 20 cm diameter telescope and onto a near infrared detector. Using the hard target we obtained very good agreement with theory. Figure 16 shows a scan of the methane line at 1650.96 nm from a 1.5 km (one way) open path and comparison with theory assuming a 1.745 ppm methane concentration.

We also demonstrated sensitive lidar measurements using a commercial photon counting detector (Hamamatsu H10330A-75). Although the quantum efficiency of the PMT is very low (< 1%) at this wavelength, it is still usable. The laser was aimed off the hard target and pointed at the side of a microwave cell phone tower. One of the wavelengths was chosen to be coincident with the absorption peak (as illustrated in

AMTD
3, 4675–4705, 2010

Fig. 16) and the other wavelength was off the absorption. Figure 17 shows the return from two closely spaced wavelengths (Online and Offline) and it clearly shows that the online wavelength experiences significant absorption whereas the offline wavelength does not.

5 Conclusions

The goal of this work was to advance the technology readiness of a breadboard instrument for future trace gas space missions. Specifically, our work is trying to address the problem of detecting methane in planetary atmospheres (including Earth) and to advance the technology readiness level (TRL) of a compact, active sensing instrument to measure trace gases.

We have generated amplifier laser radiation in the near and mid-infrared spectral regions using optical parametric amplification and demonstrated detection of CH_4, H_2O, and CO_2 in absorption cells and in an open path. We hope to demonstrate the technique from an airborne platform next year.

This work should enable a future space LIDAR instrument to map various biogenic gases from orbit on Mars. For earth, we can use the same measurement technique at 1.65 µm to map global methane levels, in order to understand climate change and the carbon cycle.

Acknowledgements. The authors thank their sponsor, Michael New, at the NASA Astrobiology Science and Technology Instrument Development Program Office and the generous support by the Internal Research and Development Program at GSFC.

AMTD
3, 4675–4705, 2010

References

Beck, J., Wan, C., Kinch, M., Robinson, J., Mitra, P., Scritchfield, R., Ma, F., and Cambell, J.: The HgCdTe electron avalanche photodiode, IEEE LEOS Newsletter, 8–12 pp., October, 2006.

Bomse, D. S. and Kane, D. J.: An adaptive singular value decomposition (SVD) algorithm for analysis of wavelength modulation spectra, Appl. Phys. B, 85, 461–466, 2006.

Christensen, T. R., Johansson, T., Åkerman, H., et al.: Thawing sub-arctic permafrost: Effects on vegetation and methane emissions, Geophys. Res. Lett., 31, L04501, doi:10.1029/2003GL018680, 2004.

Dlugokencky, E. J., Dlugokenck, S., Bruhwiler, L., et al.: Atmospheric methane levels off: Temporary pause or a new steady state, Geophys. Res. Lett., 30(19), 1992, doi:10.1029/2003GL018126, 2003.

Hamazaki, T., Kaneko, Y., Kuze, A., and Suto, H.: Greenhouse Gases Observation from Space with TANSO-FTS on GOSAT, Observation from Space with TANSO-FTS on GOSAT, OSA Fourier Transform Spectroscopy (FTS) Conference, Santa Fe, New Mexico, 11 February, 2007.

Hansen, J. E. and Sato, M. K. I.: Trends of measured climate forcing agents. P. Natl. Acad. Sci., 98, 14778–14783, doi:10.1073/pnas.261553698, 2001.

Houghton, J.: Climate Change 2001: The Scientific Basis, Cambridge Univ. Press, Cambridge, 2001.

Intergovernmental Panel on Climate Change Report (IPCC): http://www.ipcc.ch/index.htm, last access: September 2009, 2007.

Kahn, R. A., Martin, T. Z., Zurek, R. W., and Lee, S. W.: The Martian Dust Cycle, MARS, edited by: Keiffer, H. H., Jakosky, B. M., Snyder, C. W., and Matthews, M. S., Univ. of Arizona Press, Chapter 29, 1017 p., 1992.

Keppler, F., Hamilton, J. T. G., Bra, M., and Roeckmann, T.: Methane emissions from terrestrial plants under aerobic conditions, Nature, 439, 187–191, 2006.

Measures, R.: Laser Remote Sensing, John Wiley & Sons, New York, 1984.

Mumma, M. J., Novak, R. E., DiSanti, M. A., and Bonev, B. P.: A sensitive search for methane on Mars, AAS/Division for Planetary Sciences Meeting, 35, 937–938, 2003.

Mumma, M. J., Novak, R. E., DiSanti, M. A., Bonev, B. P., and Dello Russo, N.: Detection and mapping of methane and water on Mars, B. Am. Astron. Soc., 36, 1127, 2004.

AMTD
3, 4675–4705, 2010

Mumma, M. J., Villanueva, G. L., Novak, R. E., Hewagama, T., Bonev, B. P., DiSanti, M. A., Mandell, A. M., and Smith, M. D.: Strong Release of Methane on Mars in Northern Summer 2003, Science, 323(5917), 1041–1045, doi:10.1126/science.1165243, 2009.

National Research Council Decadal Survey: Earth Science and Applications from Space: National Imperatives for the Next Decade and Beyond, National Academic Press, 2007

Riris, H., Carlisle, C. B., Warren, R. E., and Cooper, D. E.: Signal-to-noise ratio enhancement in frequency-modulation spectrometers by digital signal processing, Opt. Lett., 19(2), 144, 1994.

Riris, R., Carlisle, C. B., and Warren, R. E.: Kalman filtering of tunable diode laser spectrometer absorbance measurements, Appl. Optics, 33(24), 5506, 1994.

Smith, M. D.: Spacecraft observations of the Martian atmosphere, Annu. Rev. Earth Planet. Sci., 36, 191–219, 2008.

Smith, P. H., Tamppari, L. K., Arvidson, R. E., et al.: H_2O at the Phoenix Landing Site, Science, 325, 58, 2009.

Werle, P., Mucke, R., and Slemr, F.: The Limits of Signal Averaging in Atmospheric Trace-Gas Monitoring by Tunable Diode-Laser Absorption Spectroscopy (TDLAS), Appl. Phys. B, 57, 131–139, 1993.

Werle, P., Mazzinghi, P., D'Amato, F., De Rosa, M., Maurer, K., and Slemr, F.: Signal processing and calibration procedures for in situ iode-laser absorption spectroscopy, Spectrochim. Acta A, 60, 1685–1705, 2004.

Yokota, T., Yoshida, Y., Eguchi, N., Ota, Y., Tanaka, T., Watanabe, H., and Maksyutov, S.: Global Concentrations of CO_2 and CH_4 Retrieved from GOSAT: First Preliminary Results, SOLA, 5, 160–163, 2009.

AMTD
3, 4675–4705, 2010

Table 1. LIDAR parameters used in the signal to noise ratio calculations for Mars orbit.

Parameter	Value
Peak power	5 W (nominal)
Repetition rate	5 KHz
Pulsewidth	10 ns
Orbit altitude	400 km
Ground speed	3 km/s
Laser spot diameter	100 m
Detector quantum efficiency	70%
Telescope diameter	0.5 m
Off line transmission	70%
Surface reflectivity	0.26

AMTD
3, 4675–4705, 2010

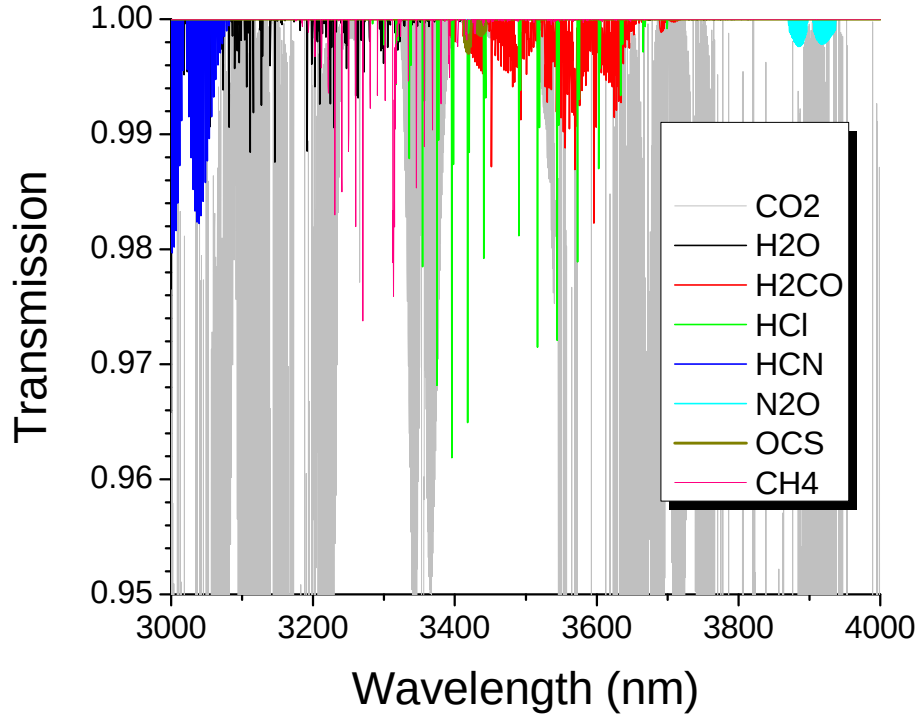

Fig. 1. One way atmospheric transmission from Mars orbit 3.0 to 4.0 µm (assuming 10 ppb mixing ratio for H_2O and 1 ppb for all other trace gases).

AMTD
3, 4675–4705, 2010

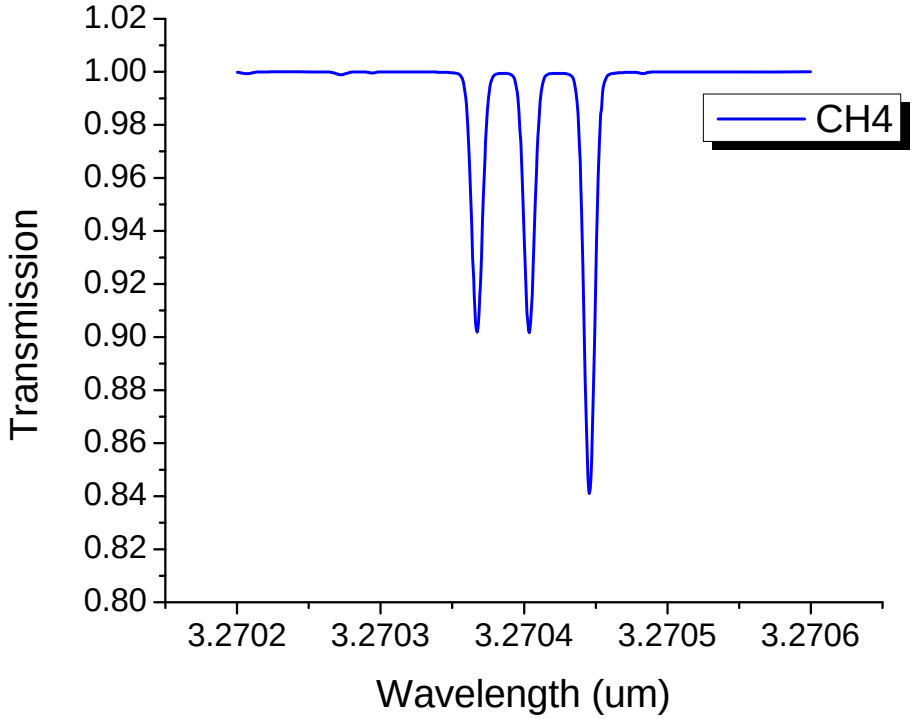

Fig. 2. Two way methane transmission spectrum from orbit in the Martian atmosphere assuming a uniform 10 ppb mixing ratio.

AMTD
3, 4675–4705, 2010

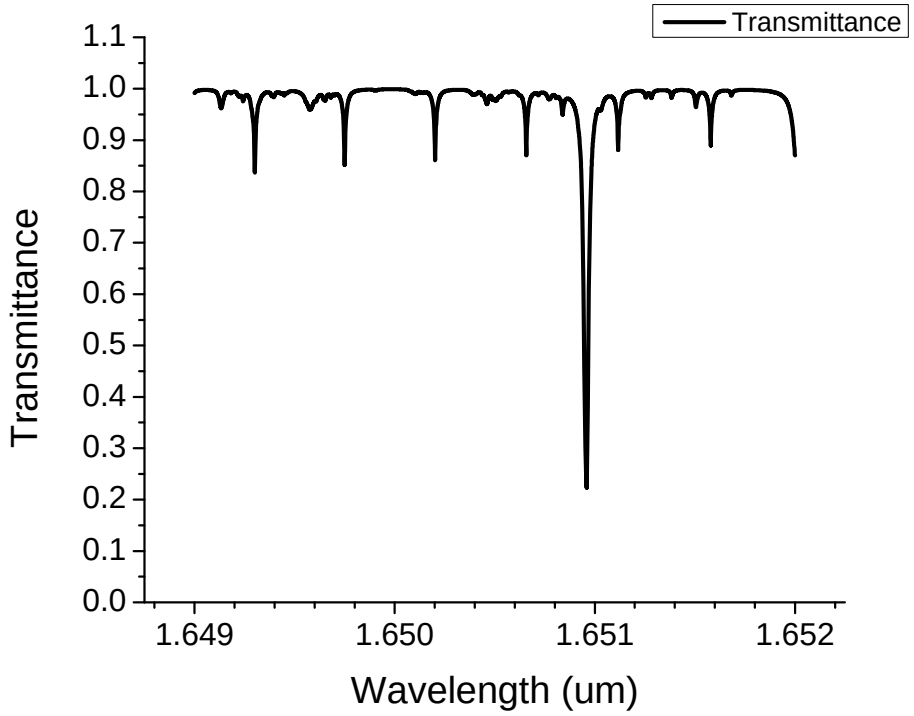

Fig. 3. One way atmospheric transmission spectrum from orbit in Earth's atmosphere showing the methane absorption line at 1.651 μm.

AMTD
3, 4675–4705, 2010

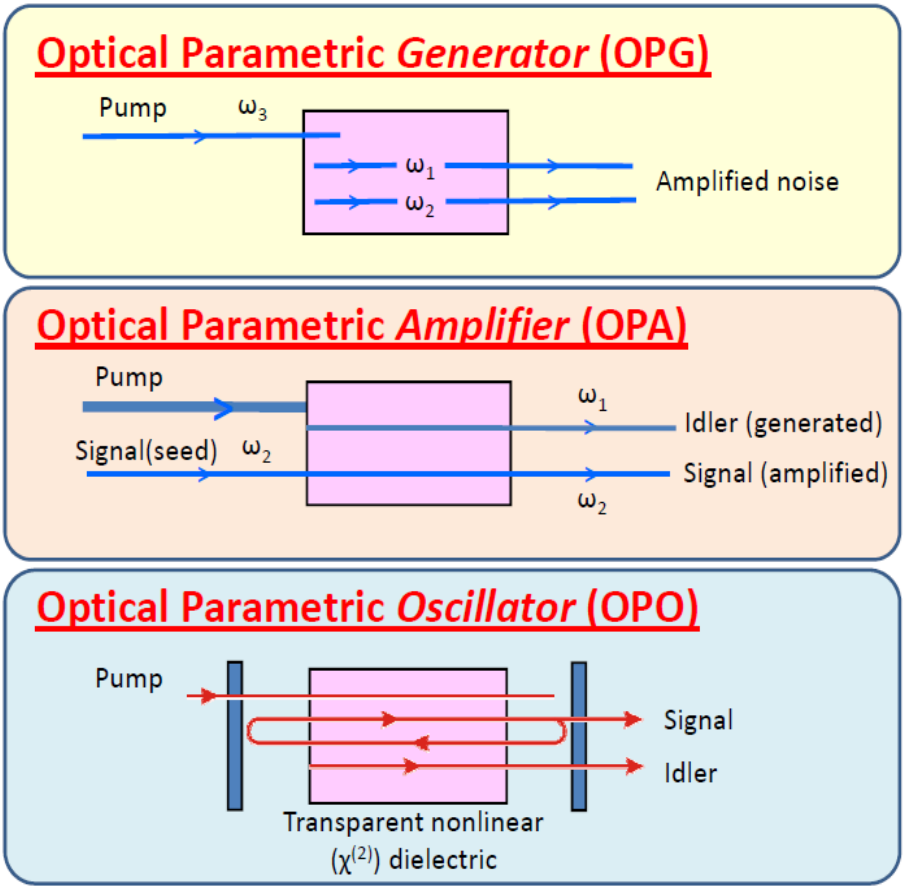

Fig. 4. Optical Parametric Generation schematic showing the differences between optical parametric amplification and optical parametric oscillator.

AMTD
3, 4675–4705, 2010

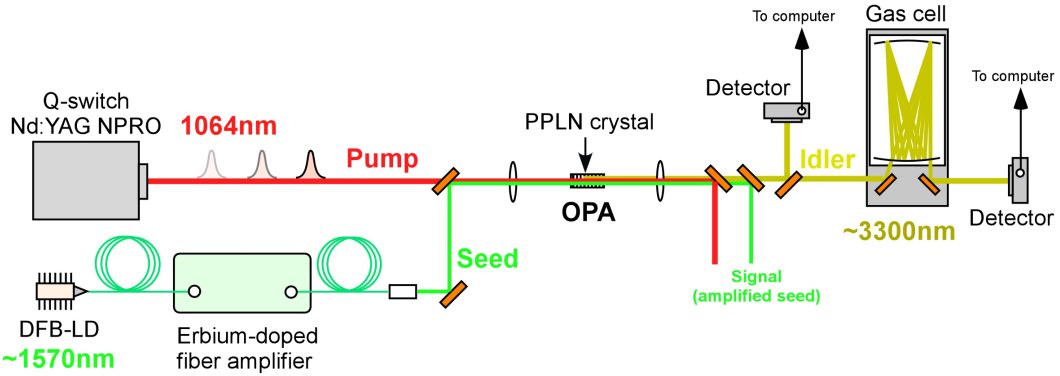

Fig. 5. Optical Parametric Amplifier (OPA) Setup at GSFC used for this work.

AMTD
3, 4675–4705, 2010

LIDAR technology for measuring trace gases on Mars and Earth

H. Riris et al.

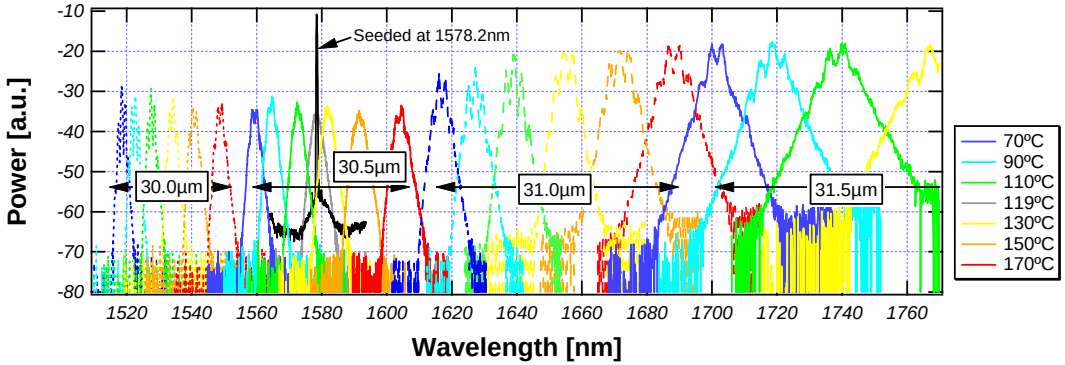

Fig. 6. Signal tuning by changing period and temperature of MgO:PPLN crystal. Unseeded OPG spectra and seeded OPG spectrum at 1578.2 nm are shown.

AMTD
3, 4675–4705, 2010

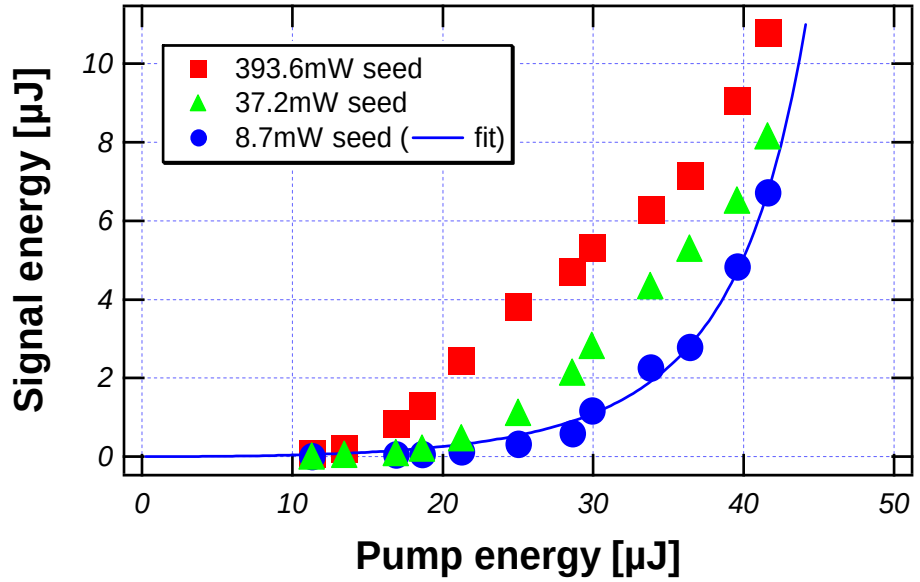

Fig. 7. Relationship between signal and pump energies at different seed power levels.

AMTD
3, 4675–4705, 2010

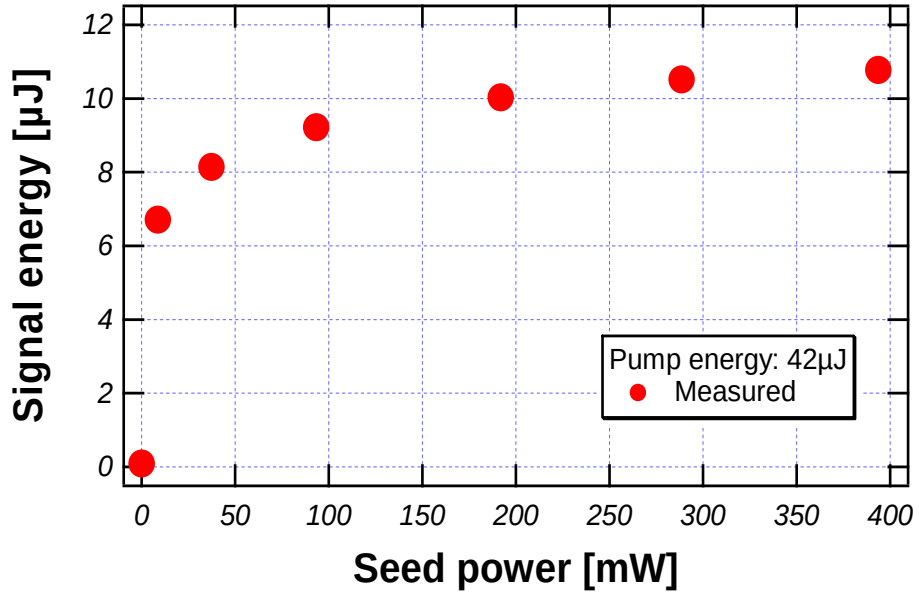

Fig. 8. Relationship between seed power vs. signal power at 42- µJ pump energy.

AMTD
3, 4675–4705, 2010

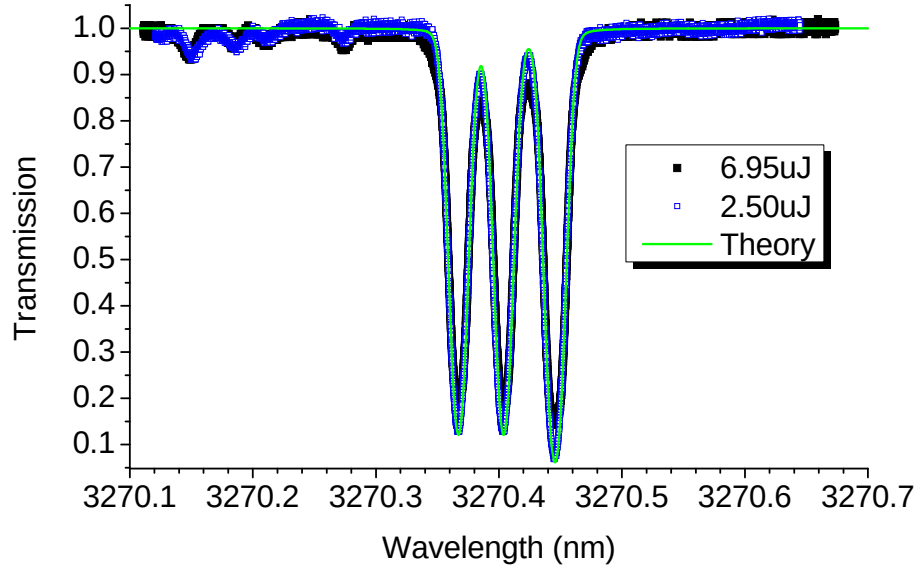

Fig. 9. Methane Spectra through an absorption cell at 3.3 µm.

AMTD
3, 4675–4705, 2010

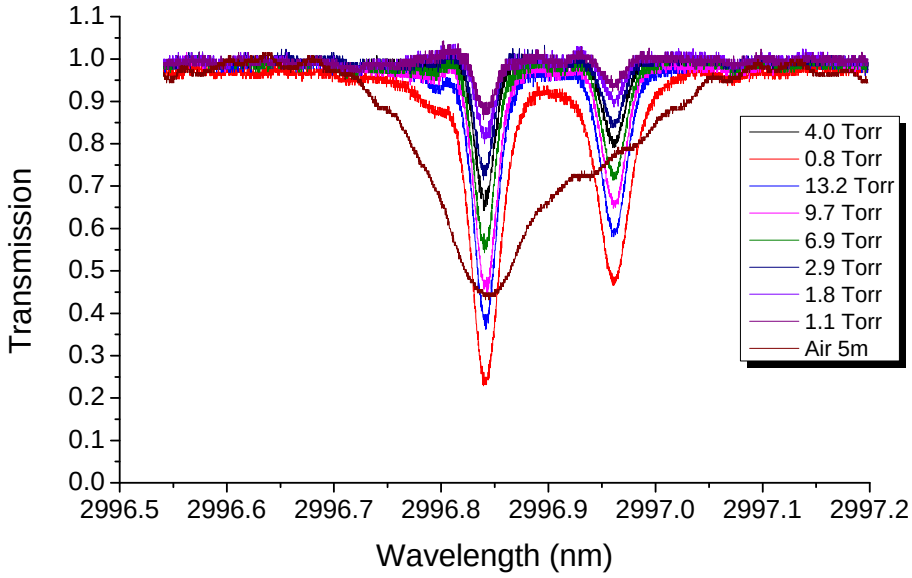

Fig. 10. Water Vapor Spectra at various pressures through an absorption cell at ~3.0 µm.

AMTD
3, 4675–4705, 2010

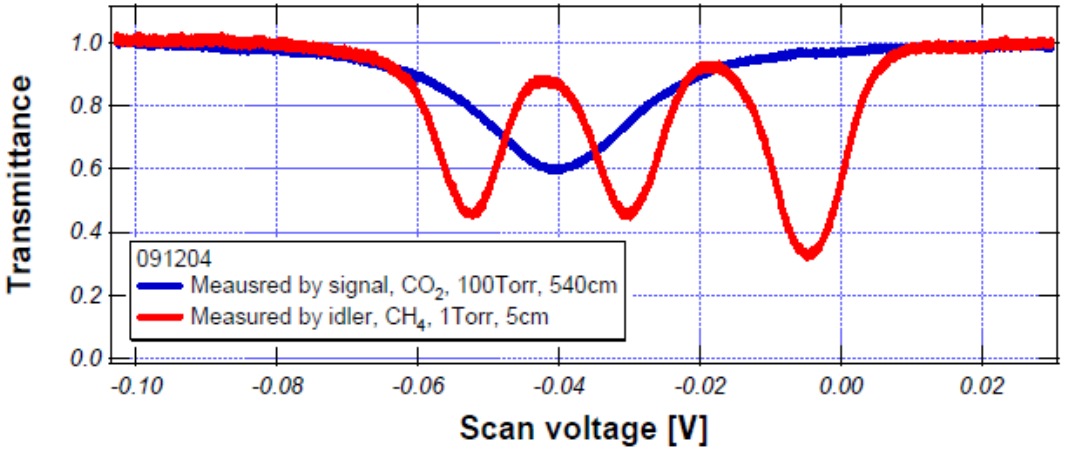

Fig. 11. Simultaneous detection of CH_4 at 3.270 µm (red) and CO_2 absorption at 1.578 µm (blue) with our OPA.

AMTD
3, 4675–4705, 2010

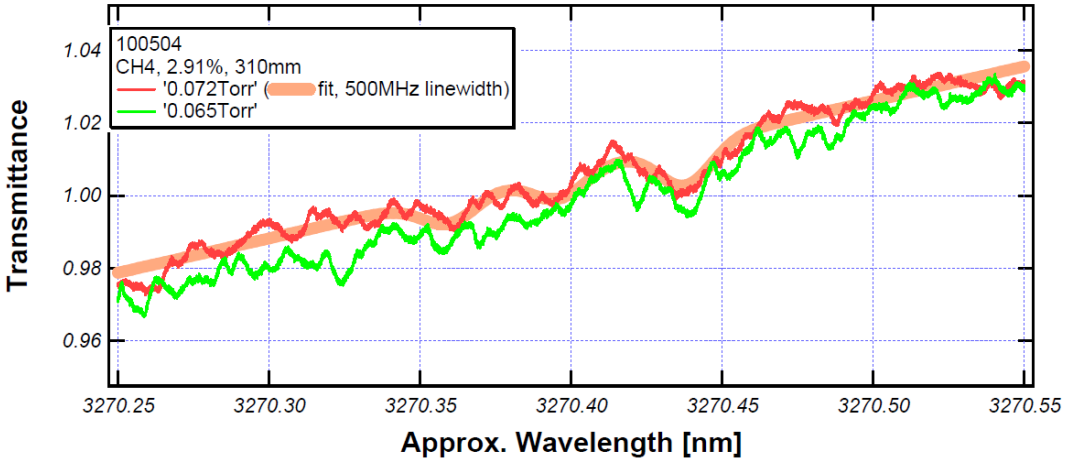

Fig. 12. Methane measurements in a cell showing the minimum detectable absorption using 2.91% methane mixture.

AMTD
3, 4675–4705, 2010

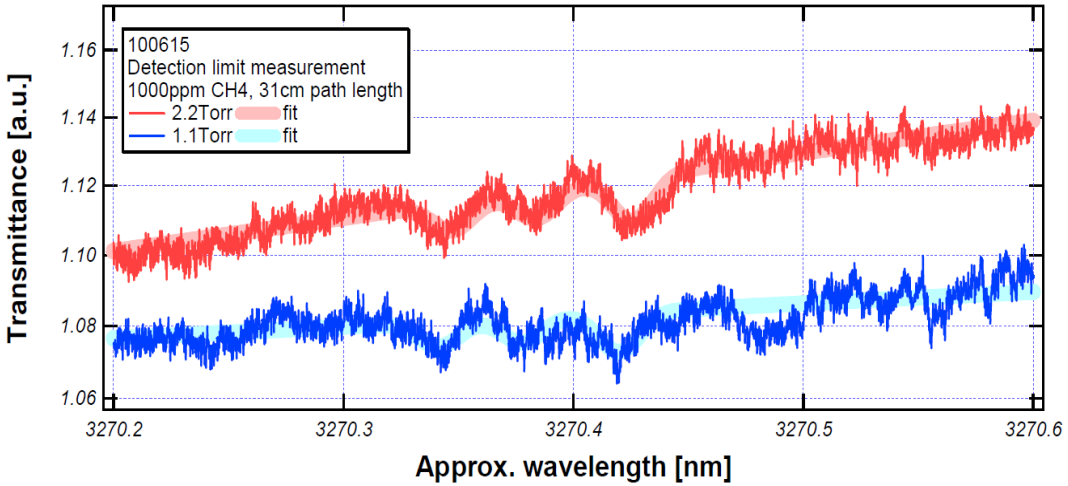

Fig. 13. Methane measurements in a cell showing the minimum detectable absorption using 1000 ppm methane mixture.

AMTD
3, 4675–4705, 2010

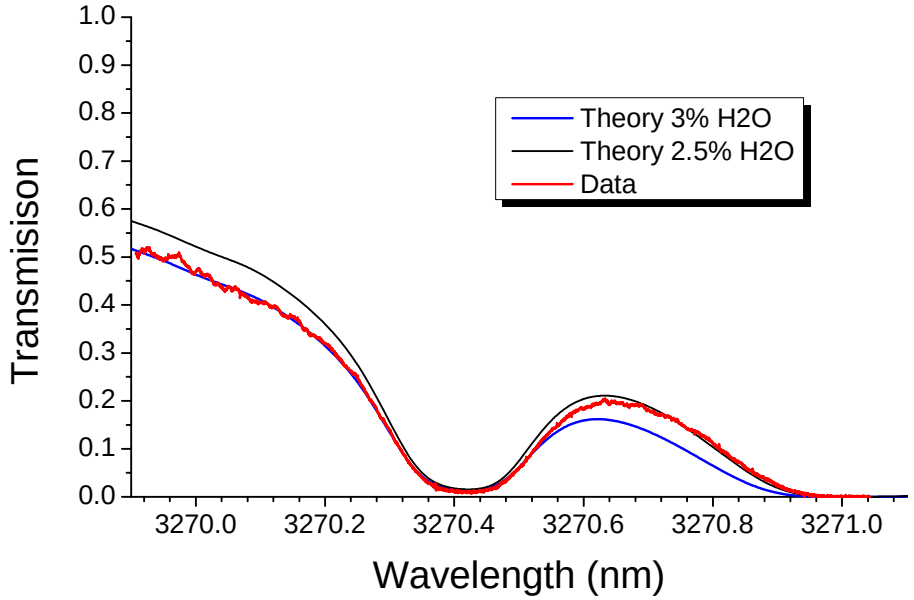

Fig. 14. Methane Spectra in a 200 m open path at 3.270 µm.

AMTD
3, 4675–4705, 2010

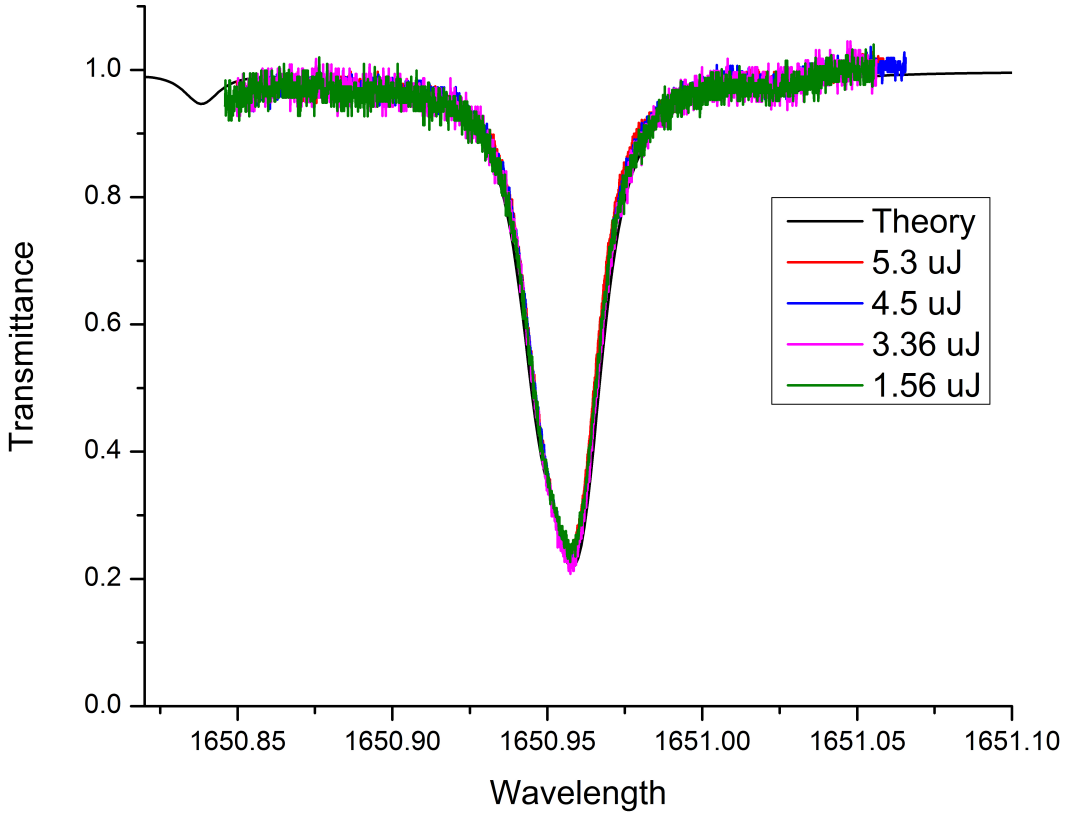

Fig. 15. Methane measurements at 1651 nm in a cell at various OPA power levels.

AMTD
3, 4675–4705, 2010

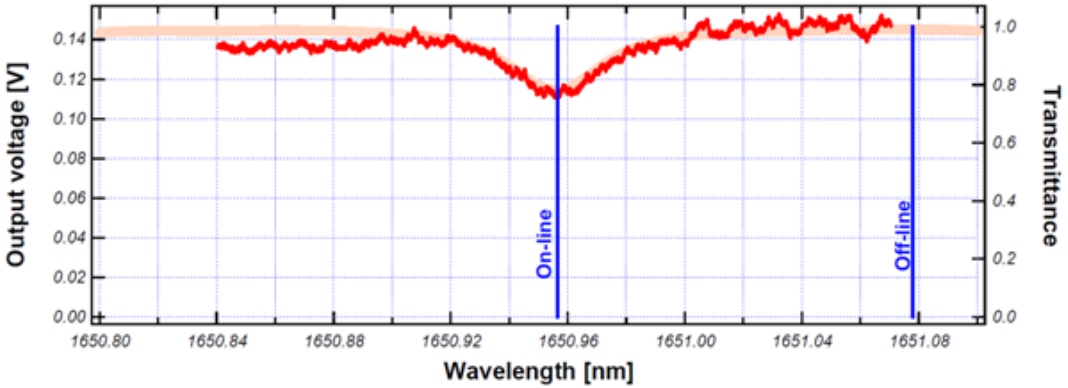

Fig. 16. Open path methane measurement at 1651 nm.

AMTD
3, 4675–4705, 2010

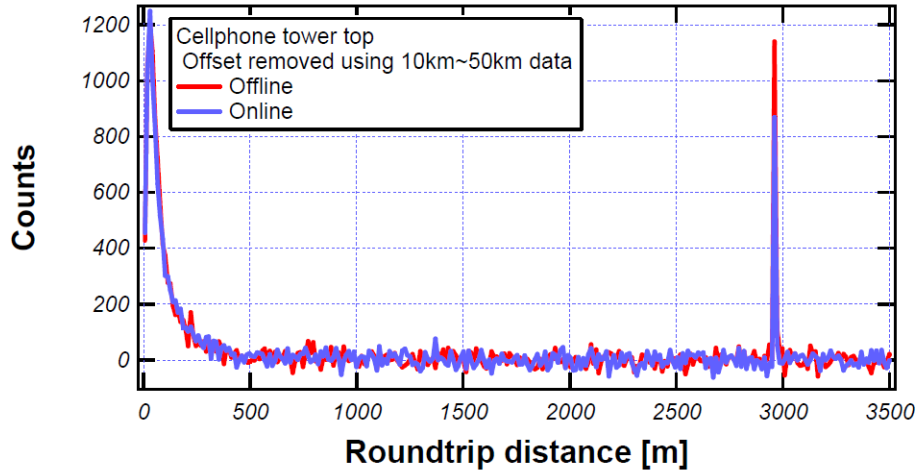

Fig. 17. Open path methane photon counting LIDAR measurements at 1651 nm.

AMTD
3, 4675–4705, 2010